# Shift of Paradigms in Understanding of Intermetallic Compounds by Analysis of Chemical Bonding within the Electron Localizability Approach

*Miroslav Kohout, Horst Borrmann, Ulrich Burkhardt, Raul Cardoso Gil, Frank Haarmann, Peter Jeglič[1], Andreas Leithe-Jasper, Takao Mori[2], Yurii Prots, Walter Schnelle, Marcus Schmidt, Olga Sichevich[3], Igor Veremchuk, Frank R. Wagner, and Yuri Grin*

The crystal structures of intermetallic compounds are often described in a traditional crystal-chemical manner as being built of structural segments having different dimensionality and periodicity, such as atomic chains (1D, one-periodic) or columns (3D, one-periodic), layers (2D, two-periodic) or slabs (3D, two-periodic), clusters (3D, zero-periodic) or frameworks (3D, three-periodic). For the majority of inorganic compounds such an interpretation is based on the understanding of atomic interactions which, in general, are different within and between the structural segments. In case of intermetallic compounds the selection of these structural segments is not obvious. They are mainly defined by geometrical factors, like axis ratio (e.g., layers are often perpendicular to the shortest lattice parameter), or from the analysis of the shortest (homoatomic or homodesmic) distances, as for boron layers in aluminium diboride $Al_{0.9}B_2$ and its derivatives.

The analysis of the chemical bonding in real space developed at the MPI CPfS (cf. chapter *Theoretical aspects of electron localizability*) opens new opportunities in understanding and description of intermetallic compounds. Several examples are discussed in the chapters *The Nature of Laves Phases and $Sr_2Ni_3$ – a Strontium Subnickelide?* Here, we present examples for which the consequent application of the electron localizability approach paves the way for a shift of paradigm in the understanding of the known structural patterns or of the well known intermetallic phases.

Electronic structure calculations were carried out using the program package TB-LMTO-ASA [1]. Details of the calculations are described in the original publications. The electron localizability indicator (ELI, $\Upsilon$) [2] was evaluated in the ELI-D representation according to Refs. [3,4]. To this end, an ELI-D module was implemented into the TB–LMTO–ASA [1] program package. It allows the calculation of the partial ELI-D contributions from different energy ranges in the electronic density of states (DOS). For isolated atoms, relativistic ZORA calculations were performed with the ADF code [5] using the TZ2P basis set. ELI-D and electron density were analyzed using the program Basin [6] with consecutive integration of the electron density in basins. These basins are bound by zero-flux surfaces in the ELI-D or electron density gradient field. In case of ELI-D such a treatment resembles the procedure proposed by F. R. W. Bader for the electron density [7].

Representatives of the structure types $YCrB_4$ and $Y_2ReB_6$ are known as crystal-chemical derivatives of the structural motif of aluminium diboride. While in $Al_{0.9}B_2$ boron atoms form planar layers of regular hexagons, in the prototype structures of $YCrB_4$ and $Y_2ReB_6$ they are arranged in planar nets of edge-condensed penta-, hexa- and heptagons (Fig. 1, top). The metal atoms are located between the boron layers (yttrium – in front of boron heptagons, transition metals – in front of boron pentagons). In this way these structural patterns are interpreted as layered segments (two-dimensional) suggesting that the atomic interactions between and within the layers are different. However, the discovery of the compound $Mg_2Rh_{1-x}B_{6+2x}$ and the analysis of the chemical bonding [8] raised first doubts in such an interpretation. It was found, that the rhodium atoms are partially replaced by boron pairs which clearly interconnect the boron nets to a 3D framework. Thus, electronically and chemically, rhodium atoms and boron pairs should play a similar role [8]. The direct confirmation of the special behavior of the transition metals in the $YCrB_4$ derivatives was obtained by the analysis of the chemical bonding in $TmAlB_4$ [9] and in the new series of compounds *RE*$RhB_4$ (*RE* = Y, Dy – Lu) [10].

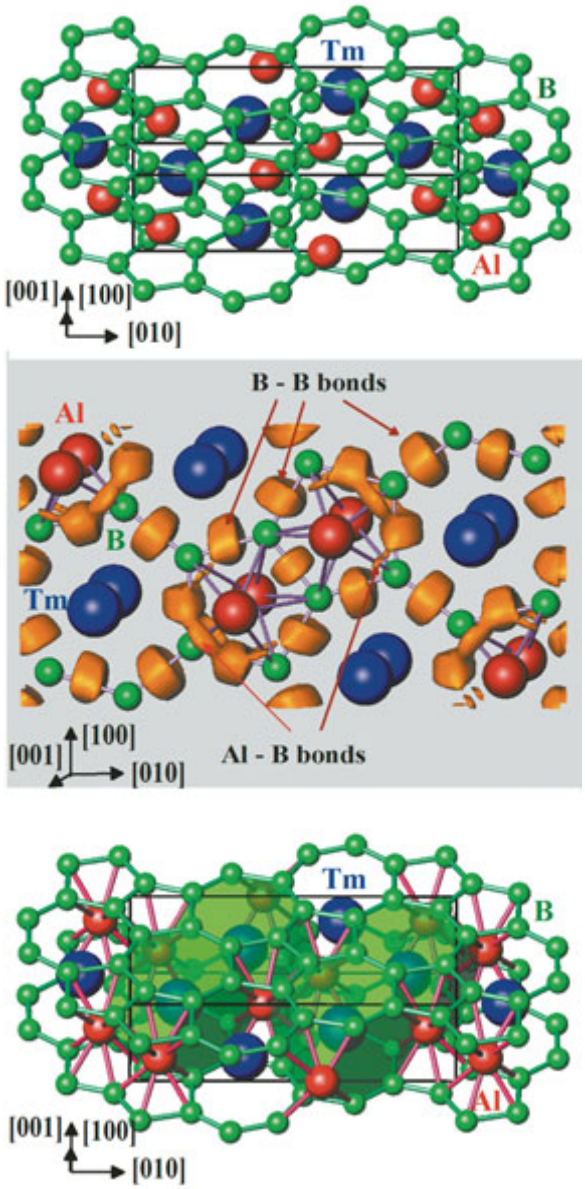


*Fig. 1: Crystal structure of $TmAlB_4$ ($YCrB_4$ structure type): (top) traditional interpretation as a stacking of planar boron layers with the metal atoms located in-between; (middle) isosurface of ELI-D ($\Upsilon_D$ = 1.65), visualizing two-center bonds between the boron atoms as well as between the aluminium and boron atoms;(bottom) quantum chemical interpretation as a 3D aluminium-boron network with Tm atoms in the cages.*

The distribution of ELI (originally, the results on the electron localization function were published [9]) reveals maxima within the boron nets as fingerprints of direct (covalent) bonding. The maxima are located between the neighbouring boron atoms, and their electron populations are 1.5 - 2.5 per bond. This suggests the formation of two-electron–two-centre bonds within the boron nets. In addition, maxima of ELI-D were found between the boron atoms of the pentagonal rings and the aluminium atoms (Fig. 1, middle), revealing a similar character of the atomic interactions within and between the planar boron nets. These findings profoundly change the understanding of the crystal structure of $TmAlB_4$: The original picture of an arrangement of distinct layers needs to be modified to one with a three-dimensional framework formed by covalently bonded boron and aluminium atoms with Tm atoms trapped in the cages of the framework (Fig. 1, bottom).

The formation of additional Al-B bonds explains the relative stability of the structural segments including the pentagonal boron rings and allows to understand the local disorder in the crystal structure which is manifested in form of microtwinning (~1 vol. %) found by precise crystal structure determination. The local disorder leads to the appearance of new atomic environments for Tm and causes complex magnetic ordering behavior (several magnetic anomalies have been observed at low temperatures) which otherwise could not be understood on the basis of a completely ordered crystal structure with one crystallographic position for the thulium atoms [9].

The findings on $TmAlB_4$ raised the question whether the formation of the three-dimensional network is a special feature of this particular compound, or a general tendency among the representatives of the $YCrB_4$ type. Further analysis was performed on the series of new compounds $RERhB_4$ (*RE* = Y, Dy – Lu), with emphasis on the Y and Yb representatives [10].

In order to shed light on the character of the interaction between the boron substructure and the metal species in the crystal structures of $YRhB_4$ and $YbRhB_4$ the charges of the QTAIM (Quantum Theory of Atoms in Molecules) atoms were calculated by integration of the total electron density within the atomic basins obtained by the topological analysis of the electronic density. Whereas the rare-earth metals clearly serve as cations ($Y^{1.62+}$ and $Yb^{1.50+}$), the Rh ($Rh^{0.1-}$) behaves more similar to boron (calculated charges are between $B^{0.13-}$ and $B^{0.65-}$). Already the fact that the charge transfer from rhodium to the boron network is around zero suggests covalent bonding in this region in agreement with the small electronegativity difference between boron and rhodium. In the topology of ELI-D, this interaction is manifested not by forma-

tion of a designated ELI-D attractor, as usually done in the ELI representation, but in the structuring of the penultimate shell (Fig. 2, middle and bottom) [11,12]. A merely 'flat' region of ELI-D is observed on the Rh-B contacts at the positions where separated attractors may be expected, as it was found between the Al and B positions in $TmAlB_4$. This observation is in agreement with the previous bonding analyses for the intermetallic rhodium compounds $RhBi_4$ [13], $Rh_3Bi_{14}$, $RhBi_{12}Br_2$ [14], $Rh_4Ga_{21}$ and $Rh_3Ga_{16}$ [15], where either less pronounced attractors or mere structuring of the penultimate Rh shell were found as fingerprints for the Rh-Bi or Rh-Ga interactions. The

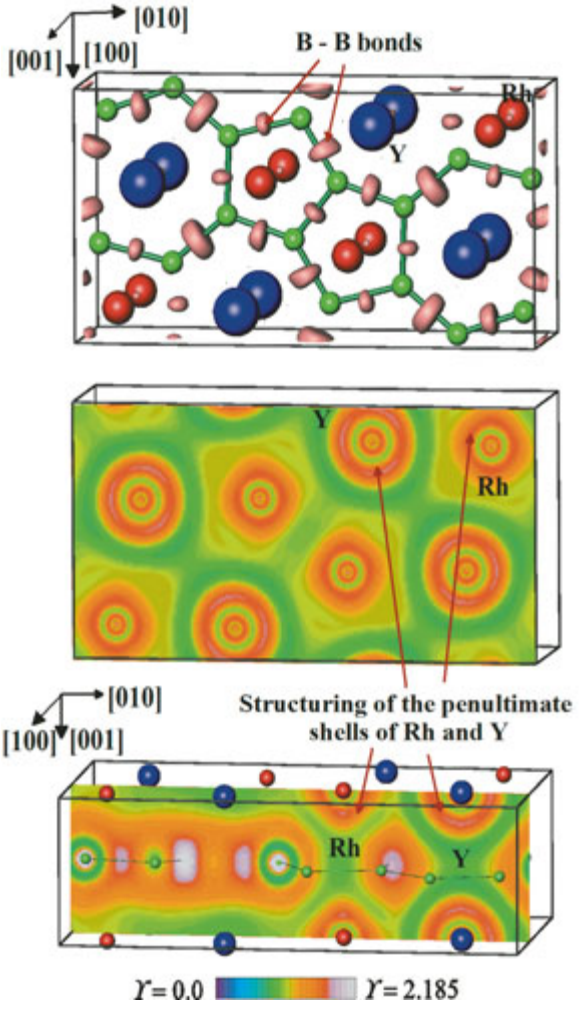


*Fig. 2: Electron localizability indicator in $YRhB_4$ ($YCrB_4$ structure type): (top) isosurface of ELI-D ($\Upsilon_D$ = 1.73), visualizing two-center bonds between the boron atoms in the planar nets; (middle) ELI-D distribution in the (001) plane; (bottom) ELI-D distribution in the plane at x = ¾. The structuring of the penultimate shells of yttrium and rhodium indicates their participation at the interactions in the valence region forming the 3D $[RhB_4]$ polyanion.*

direct boron-boron bonds are clearly visualized by ELI-D (Fig. 2, top).

Thus, $YRhB_4$ and $YbRhB_4$ can be described as a covalently bonded 3D polyanion containing planar nets of threefold bonded boron atoms interconnected by rhodium atoms with the Y or Yb cations captured in the cavities of the polyanion. Such an electronic structure of the polyanionic network appears to be very stable: the boron-boron distances do not vary noticeably for different *RE* components. However, there is no correlation between the B–B bond length and the respective electron population of the according basin in the ELI representation.

The heavier homologues of boron—aluminium and gallium—rarely form intermetallic compounds which are isotypic with the boron representatives. Rather, they often result in compounds with a similar topology of the lattice. In particular, the compounds with high Ga (Al) content are often interpreted as layered. This applies to the representatives of the structure type $CeFe_2Al_8$. The orthorhombic crystal structure has one relatively short lattice parameter and is traditionally described with two different types of flat layers perpendicular to [001]. In case of the recently investigated compounds $EuT_2Ga_8$ ($T$ = Co, Rh, Ir), one layer contains only gallium atoms, the second one is occupied by gallium, rhodium and europium (Fig. 3, top).

Striking features of the ELI-D diagram are the spherical regions of high ELI-D values around the atomic nuclei, highlighting the atomic shell structure, as well as the ELI-D maxima between the Ga atoms forming pentagonal prisms centered by the Eu atoms. The latter can be seen as a signature of the covalent bonding between the Ga atoms, similar to the boron-boron bonds in $TmAlB_4$ or $RERhB_4$ above.

Analogous to the boron compounds, the penultimate ELI-D shells of Rh (fourth shell) and Eu (fifth shell) are structured (Eu – strongly, Rh – less), i.e., they deviate from spherical symmetry which is characteristic for non-interacting isolated atoms. This was quantified by the structuring index ε (ε is the difference between the highest ELI-D value in the examined shell and the ELI-D value at which the localization domain is without a 'hole' [12]). The respective indices for ELI-D are ε_Rh = 0.04 (fourth shell, average for two atoms) and ε_Eu = 0.40 (5$^{th}$ shell) compared to an average

ε_Ga = 0.015 for the third shells of the Ga atoms. Structuring of the inner ELI-D shells is shown to be an indication for their participation in the bonding [11,12].

ELI-D points to the presence of attractors in the vicinity of the Rh and Ga atoms. Either ring-shaped localization domains are observed, or the attractors are located within the gallium shell around the rhodium atoms. The localization domains for these attractors are grouped around the Ga atoms. Additional ELI-D attractors are found between the Ga atoms forming pentagonal prisms. Altogether, the Rh and Ga atoms form a network polyanion with (possibly) polar covalent bonds. The polar character of these bonds is characterized by the charge transfer between the QTAIM Rh and Ga atoms. Europium species are located in the cavities of the polyanion. The integration of the electron density within the four inner ELI-D shells of the Eu species (atomic core) yields a charge transfer of 1.6 electrons to the Rh-Ga network and reveals an ionic interaction between the europium cation and the [$Rh_2Ga_8$] polyanion. However, the observed charge transfer is less than the 1.9 electrons in the valence shell determined from the ELI-D distribution for a free Eu atom. This, together with the structuring of the fifth ELI-D shell of Eu in $EuRh_2Ga_8$, points towards an additional bonding interaction between Eu and the Rh-Ga network. A more detailed analysis of this interaction is conducted by means of the partial ELI-D contributions.

ELI-D can be seen—in a simplistic view—as a charge needed to form a fixed fraction of an electron pair. It is given by the product of the electron density and the volume required by that pair fraction (so called pair-volume function) [16]. Now, the charge can be decomposed into contributions, for instance from states belonging to a certain energy range in the electronic DOS. The product of such density contributions and the corresponding pair-volume function yields the contribution of the particular energy range to the total ELI-D, the so-called partial ELI-D [12,17]. Of course, in this representation the sum of all partial ELI-D contributions must yield the total ELI-D, in the same way as the sum of all partial electron density contributions must result in the total electron density. Thus, such a decomposition of ELI-D into contributions is exact and consistent.

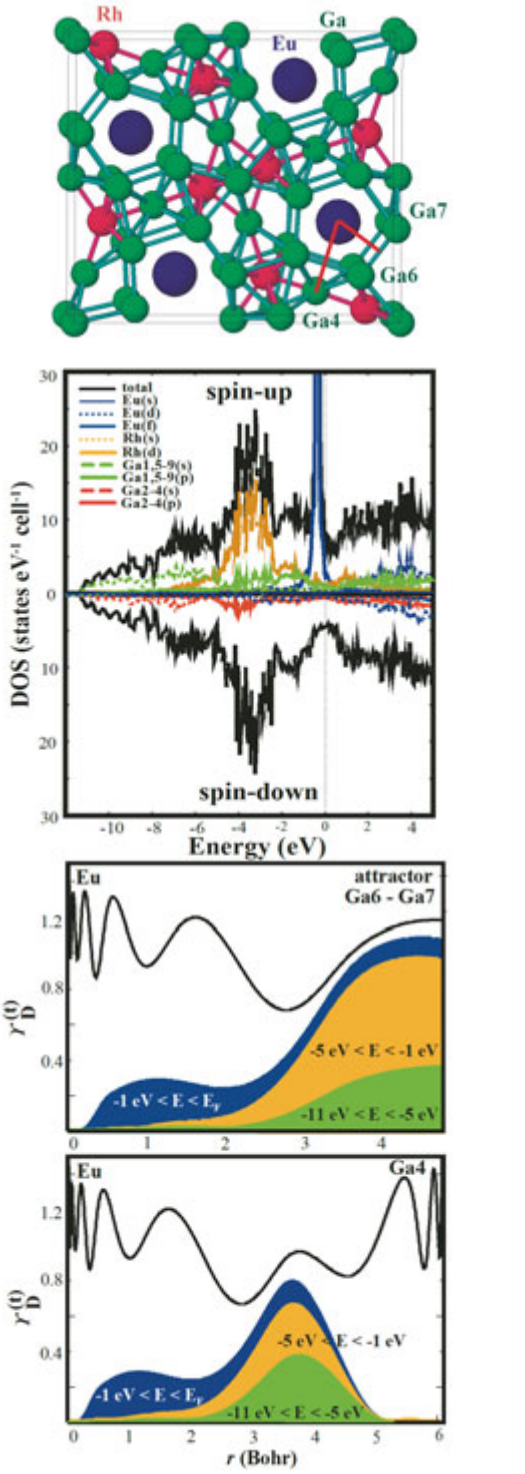


*Fig. 3: Crystal structure and bonding in $EuRh_2Ga_8$: (top) atomic layers and shortest Ga-Ga (green) and Rh-Ga (pink) contacts in projection along [001]; (middle) electronic DOS with partial contributions of atomic states; (bottom) ELI-D distribution along the lines given in red in the top figure – total ELI-D (black) with partial contributions of different energy regions of the DOS. The latter visualize the contributions of the electrons of the penultimate shells of Eu and Rh in the boding interactions in the valence region.*

For the analysis the contributions of three different regions were computed, –11 eV ≤ $E$ ≤ –5 eV, –5 eV ≤ $E$ ≤ –1 eV, and –1 eV ≤ $E$ ≤ $E_F$, respectively (cf. electronic DOS in Fig. 3, middle). The states from the lowest (valence) energy range (contributions of Ga atomic states) participate in ELI-D mainly (around 50%) between the Ga atoms as well as in the outer regions of the Ga prisms. The partial ELI-D contributions from the second energy range (atomic Rh(*d*) and Ga(*p*) levels) indicate that the ELI-D maxima between Rh and Ga result to a large extent from the interaction between these atomic levels (around 50% participation, cf. line Eu – attractor of the Ga6-Ga7 bond in Fig. 3, bottom). The partial ELI-D computed from the states within the highest energy range (1 eV below the Fermi level) nicely confirms that the structuring of the fifth Eu shell is due to the *f* states. In addition, it reveals the clear participation of the Eu(*f*) states in the bonding interaction towards the Rh or Ga atoms of the equatorial ring of the coordination sphere of Eu (Fig. 3, bottom, Eu-Ga4 line). Thus, both lines above visualize the interaction between Eu and the [$Rh_2Ga_8$] polyanion. In both cases, the contributions of the highest energy range of the DOS to the ELI-D in the bonding region are remarkably large: in case of the Eu – Ga4 line, the contribution is around 17%, in case of the line Eu – attractor Ga6-Ga7 it is 12%.

In total, despite the pronounced layered appearance of the crystal structure, the chemical bonding analysis for $EuRh_2Ga_8$ reveals the formation of a 3D [$Rh_2Ga_8$] polyanion by Ga-Ga and polar Rh-Ga bonds. Europium shows two types of interactions with the polyanion. The first one is more of ionic nature with a charge transfer from europium to the Ga-Ga bonds in the first coordination shell. The second type is caused by participation of the electrons of the fifth shell of europium in the bonding (mainly in the equatorial plane of the coordination sphere, layer two above with mixed occupation).

The compound o-$Co_4Al_{13}$ attracts special attention because of its structural features. Although its unit cell is relatively small in comparison with other representatives of the complex metallic alloy phases family (CMA, cf. chapter *Complex Metallic Alloys*), the crystal structure possesses all characteristics of a CMA: large number of atoms in the unit cell, local atomic disorder, and atomic arrangements with pseudo-pentagonal symmetry [18]. The crystal structure of o-$Co_4Al_{13}$ is traditionally

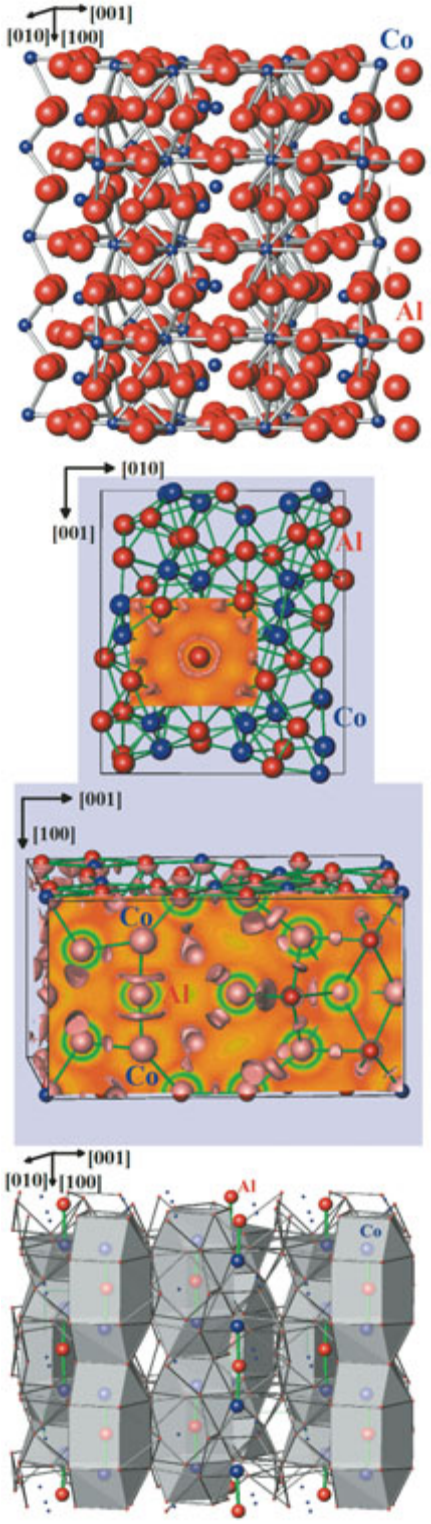


*Fig. 4: o-$Co_4Al_{13}$ - from an approximant to a cage compound: (top) atomic layers along [100] and the shortest Co-Al contacts; (middle, upper part) ELI distribution between the layers visualizing the covalently bonded Co-Al 3D framework; (middle, lower part) ELI distribution at y ≈ 0.75 revealing formation of the covalently bonded Co-Al-Co groups; (bottom) clathrate-like organization of the crystal structure as obtained from the bonding analysis.*

interpreted as comprising atomic layers perpendicular to [100]. Due to the (pseudo) penta- and decagonal arrangements of the atoms within these layers, o-$Co_4Al_{13}$ is considered as one of the simplest approximants to the decagonal quasicrystals.

For detailed structural investigation and measurements of physical properties, high-quality single crystals of o-$Co_4Al_{13}$ were prepared by Bridgman and Czochralski methods in the groups of Prof. P. Gille (LMU, München) and Dr. M. Feuerbacher (FZ Jülich) within the European Network of Excellence 'Complex Metallic Alloys'. A high-resolution investigation of the crystal structure was performed at the MPI CPfS using X-ray diffraction data set with $2\theta < 123°$ (AgKα radiation). All cobalt positions were found to be fully occupied, whereas the aluminium sites revealed positional disorder in distinct regions of the crystal structure. Resolving this disorder yielded three equivalent models all of which represent distortion variants of the pseudo-pentagonal columnar structural units characteristic for this group of CMA [19].

The analysis of the chemical bonding in the ordered models by means of the electron localizability indicator led to a highly unexpected result. Numerous directed (covalent) Co-Al and Al-Al bonds were found within the atomic layers perpendicular to [100] as well as in-between the layers (Fig. 4 top and middle) revealing the formation of a 3D framework, contrary to the traditional consideration in terms of atomic layers. In addition, in the elongated cavities parallel to [100], isolated three-atomic groups Co-Al-Co were found. From the topology of ELI-D, the atomic interactions within the group (directed, covalent) differ from those between the group and the atoms of the framework (non-directed, ionic). This unusual feature reveals a surprising analogy between o-$Co_4Al_{13}$ and intermetallic clathrates (cf. chapter *Intermetallic Clathrates Revisited*). Their crystal structures also exhibit covalently bonded 3D networks with filler atoms in the cavities, interacting ionically with the host framework.

Despite the complexity of the crystal structure the NMR spectroscopic experiments (Fig. 5) confirmed the results of the bonding analysis and strongly supported the unique bonding situation of Al in nearly linear Co-Al-Co groups [20].

In addition, the developed bonding model was supported by the results of measurements of the electrical conductivity and specific heat on oriented single crystals conducted in cooperation with the group of Prof. J. Dolinšek (JSI, Ljubljana) [21]. Structure investigations of the (100) surface of a single crystal of o-$Co_4Al_{13}$ by STM are in full agreement with the conclusions of the bonding analysis. They were performed in the group of Prof. J.-M. Dubois (CNRS, Nancy) [22].

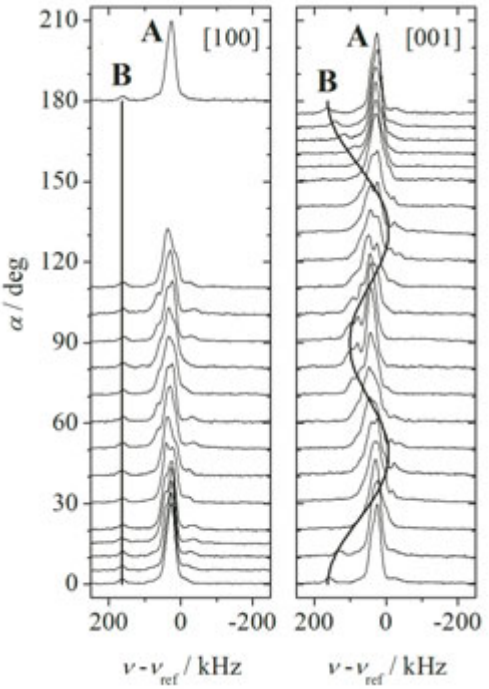


*Fig. 5: $^{27}$Al NMR spectroscopic evidence of two different kinds of Al atoms in o-$Co_4Al_{13}$. The majority signal A reflects the Al framework atoms, the minority signal B represents the Co-Al-Co groups. The shift of the signal B by rotation of the single crystal around [001] (right) and constant behaviour by rotation around [100] (left) are in agreement with the orientation of the Co-Al-Co group along [100].*

In conclusion, applying the quantum theoretical analysis of chemical bonding within the electron localizability approach on intermetallic compounds led to a substantial or complete revision of the understanding of their structural features. The representatives of the structure type $YCrB_4$, traditionally viewed as layered compounds are shown to form 3D covalently bonded frameworks ($TmAlB_4$). The electrons of the penultimate shells of the transition metal atoms play an important role in the stabilization of the 3D polyanionic frameworks ($YRhB_4$). The rare-earth metals do not only feature cationic counterparts to the framework polyanions, but also exhibit partially covalent interactions employing the electrons of the

penultimate shells. Such a new view on bonding interactions leads to a shift of paradigm in understanding of the crystal structures and opens new opportunities for the interpretation of the physical properties.

## References


[1] *O. Jepsen, A. Burkhardt, O. K. Andersen,* The Program TB-LMTO-ASA. Version 4.7. Max-Planck-Institut für Festkörperforschung, Stuttgart, 1999.

[2] *M. Kohout,* Int. J. Quantum Chem. **97** (2004) 651.

[3] *M. Kohout, F. R. Wagner, and Yu. Grin,* Int. J. Quantum Chem. **106** (2006**)** 1499.

[4] *M. Kohout,* Faraday Discuss. **135** (2007) 43.

[5] *ADF 2007.01, SCM, Vrije Universiteit Amsterdam, The Netherlands, 2007.*

[6] *M. Kohout,* Basin, Version 4.3, 2008.

[7] *R.F.W. Bader,* Atoms in Molecules: A Quantum Theory, Oxford University Press, Oxford, 1999.

[8] *A. M. Alekseeva, A. M. Abakumov, P.S. Chizhov, A. Leithe-Jasper, W. Schnelle, Yu. Prots, J. Hadermann, E. V. Antipov, and Yu. Grin,* Inorg. Chem. **46** (2007) 7378.

[9] *T. Mori, H. Borrmann, S. Okada, K. Kudou, A. Leithe-Jasper, U. Burkhardt, and Yu. Grin,* Phys. Rev. B **76** (2007) 064404.

[10] *I. Veremchuk, T. Mori, Yu. Prots, W. Schnelle, A. Leithe-Jasper, and Yu. Grin,* J. Solid State Chem. **181** (2008) 1983.

[11] *M. Kohout, F. R. Wagner, Yu. Grin,* Theor. Chem. Acc. **108** (2002) 150.

[12] *F. R. Wagner, V. Bezugly, M. Kohout, and Yu. Grin,* Chem. Eur. J. **13** (2007) 5724.

[13] *Yu. Grin, U. Wedig, and H. G. von Schnering,* Angew. Chem. Int. Ed. Engl. **34** (1995**)** 1204.

[14] *Q. F. Gu, G. Krauss, Yu. Grin, W. Steurer,* J. Solid State Chem. **180** (2007) 940.

[15] *M. Boström, Yu. Prots, Yu. Grin,* J. Solid State Chem. **179** (2006) 2472.

[16] *M. Kohout, F. R. Wagner, Yu. Grin. J. Phys. Chem. A **112** (2008) 9814.*

[17] *E. Dashjav, Yu. Prots, G. Kreiner. W. Schnelle, F. R. Wagner, R. Kniep,* J. Solid State Chem. **181** (2008) 3121.

[18] *Yu. Grin, U. Burkhardt, M. Ellner, and K. Peters,* J. Alloys Compd. 2**06** (1994) 243.

[19] *Yu. Grin, B. Bauer, U. Burkhardt, R. Cardoso-Gil, J. Dolinšek, M. Feuerbacher, P. Gille, F. Haarmann, M. Heggen, P. Jeglič, M. Müller, S. Paschen, W. Schnelle, S. Vrtnik.* EUROMAT 2007: European Congress on Advanced Materials and Processes. Book of Abstracts, Nürnberg, Germany, 2007, p. 30.

[20] *P. Jeglič, M. Heggen, M. Feuerbacher, B. Bauer, P. Gille, and F. Haarmann,* J. Alloys Compd. (2009) in press.

[21] *J. Dolinšek, M. Komelj, P. Jeglič, S. Vrtnik, D. Stanić, P. Popčević, J. Ivkov, and A. Smontara,* Z. Jagličić, P. Gille, Yu. Grin. (2009) submitted.

[22] *R. Addou, E. Gaudry, T. Deniozou, M. Heggen, M. Feuerbacher, P. Gille, R. Widmer, O. Gröning, Yu. Grin, V. Fournée, J.-M. Dubois, and J. Ledieu.* (2009) submitted.


---

[1] Present address: Jožef Stefan Institute, Ljubljana, Slovenia.

[2] Present address: National Institute for Materials Science, Tsukuba, Japan.

[3] Present address: National University of Forestry and Wood Technology, Lviv, Ukraine.